Ab Initio Calculations and Modeling of Three-Dimensional Adiabatic and Diabatic Potential Energy Surfaces of $Br(^2P)\cdots H_2(^1\Sigma^+)$ Pre-Reactive Complex

Jacek Kłos[†] and Grzegorz Chałasiński*[,‡]

Faculty of Chemistry, University of Warsaw, Pasteura 1 02-093 Warsaw, Poland

M. M. Szczęśniak[§]

Department of Chemistry, Oakland University, Rochester, Michigan 48309

Received: February 25, 2002; In Final Form: May 13, 2002

The three lowest diabatic potential energy surfaces for the $Br(^2P) + H_2$ van der Waals complex are derived from accurate ab initio calculations of the T-shaped (C_{2v}) and collinear geometries ($C_{\infty v}$), at the coupled cluster with single, double, and noniterative triple excitations (CCSD(T)) level of theory with a large basis set. For the intermediate geometries, the angular dependence is modeled by a simple Legendre-polynomial interpolation. The nonadiabatic coupling (off-diagonal derivative) matrix element and the fourth, off-diagonal, diabatic surface are determined by separate complete active space self-consisted field (CASSCF) calculations with a medium-sized basis set. Three adiabatic potential energy surfaces (PESs) are also obtained, by diagonalizing the total Hamiltonian in the diabatic basis. Both the nonrelativistic and relativistic (including spin−orbit coupling) PESs are evaluated. The dependence of the PESs on the H_2 stretching coordinate is also incorporated and analyzed.

I. Introduction

In recent years, there has been considerable theoretical interest in electronically nonadiabatic effects in chemical reactions, and hydrogen abstraction reaction by a halogen atom, $Hal + H_2 \rightarrow HalH + H$, has been one of the most important paradigm.[1−8] Whereas the major thrust went into the investigation of $F + H_2$ and $Cl + H_2$, less is known about $Br + H_2$, especially on the experimental side. For this system, the reaction engaging the spin−orbit excited-state $Br(^2P_{1/2})$ is very interesting because the energy difference between $Br(^2P_{1/2})$ and $Br(^2P_{3/2})$ is very large (0.455 eV), unlike for related F or Cl atom. This energy splitting is close to the energy difference between $H_2(\nu = 0)$ and $H_2(\nu = 1)$ (0.512 eV), where ν is the vibrational quantum number. Because the electronic-to-vibrational energy transfer occurs in the entrance channel, it seems important to have a detailed knowledge of the van der Waals forces that determine the potential energy surface in this region. The role of weak interactions at the outset of chemical reactions has been recently emphasized by several authors.[9−11] In this paper, following our studies of the related $F + H_2$ and $Cl + H_2$ complexes,[1,2] we present ab initio calculations and modeling of the $Br + H_2$ van der Waals complex.

Pioneering theoretical work carried out by Truhlar and coworkers[5−7] focused on the reactive region and did not consider the van der Waals fragments of the potentials. The authors developed 2×2 diabatic potential energy surfaces and then carried out converged quantum reactive scattering calculations for zero total angular momentum, using the outgoing wave variational principle. They found that the quenching of the spin−orbit excited Br with the ground-state H_2 mainly produces H_2 with one quantum of vibrational excitation in the total energy range they studied. This means that the quenching process satisfies a near-resonance condition for the electronic-to-vibrational energy transfer.

On the experimental side, Nesbitt and Leone[12] reported interesting experimental results for the $Br-H_2$ system. They concluded, from their systematic laser photolysis study, that $Br(^2P_{1/2}) + H_2$ ($\nu = 1$) is efficiently quenched to $Br(^2P_{3/2}) + H_2$ ($\nu = 2$) in the entrance channel, followed by a subsequent H atom abstraction from vibrationally exited H_2

$$Br(^2P_{1/2}) + H_2\ (\nu = 1) \rightarrow [Br(^2P_{3/2})H_2\ (\nu = 2)] \rightarrow HBr + H.$$

Very recently, Takayanagi and Kurosaki[13] have performed three-dimensional quantum scattering calculations for the electronically nonadiabatic $Br(^2P_{1/2}) + H_2$ reaction. A detailed analysis of the calculated probabilities confirmed that the electronically nonadiabatic transitions from $Br(^2P_{1/2}) + H_2(\nu)$ to $Br(^2P_{3/2}) + H_2(\nu + 1)$ effectively occur in the entrance region of the potential surface. However, the contribution of the electronically nonadiabatic chemical reaction, $Br(^2P_{3/2}) + H_2(\nu) \rightarrow HBr + H$, is small.

The above nonadiabatic process of electronic-to-vibration energy transfer is possible because of the weak interaction with the H_2 molecule. The latter lifts the symmetry ban for the intramultiplet transition, and accepts the released energy. The intramultiplet mixing dynamics that is triggered by the van der Waals interaction is still a virgin area, despite recent theoretical progress achieved for the collisions of rare gas atoms with Cl,[14] O,[15] and S.[16]

* To whom correspondence should be addressed. E-mail: chalbie@chem.uw.edu.pl.

[†] Present address: Institute of Theoretical Chemistry, NSRIM, University of Nijmegen, Toernooiveld 1, 6525 ED Nijmegen, The Netherlands. E-mail: jakl@theochem.kun.nl.

[‡] Also at Department of Chemistry, Oakland University, Rochester, MI 48309.

[§] E-mail: maria@ouchem.chem.oakland.edu.

10.1021/jp020529d CCC: $22.00
Published on Web 07/13/2002

The goal of this paper is to provide accurate nonrelativistic and relativistic ab initio potential energy surfaces (PESs) for the first three states of Br + H_2 in the entrance channel fragment. These three states arise from the interaction of H_2 with the triply degenerate ^{2}P Br atom. The electron configuration of Br gives rise to $^2\Sigma^+$ and $^2\Pi$ states in the $C_{\infty v}$ configuration, to $^2A_1$, $^2B_1$, $^2B_2$ states in the triangular C_{2v} geometry, and to $1^2A'$, $2^2A'$, and $^2A''$ states in C_s geometries. The PESs are derived within the recently proposed combined ab initio coupled-cluster and model treatment, termed coupled-cluster-model (CC-M).[1,2]

The essence of the CC-model approach is to calculate accurate coupled cluster with the single, double, and noniterative triple excitations (CCSD(T)) interaction energies only for two highly symmetrical configurations, the C_{2v} and $C_{\infty v}$ geometries, and then model the three lowest diabatic surfaces of the C_s symmetry by means of a simple angular interpolation. The method proved successful for the F + H_2[1] and Cl + H_2[2] systems. The approach takes advantage of the oblate shape of the H_2 molecule, causing a relatively simple anisotropy of the interaction. To obtain the nonadiabatic coupling element of the Hamiltonian matrix (related to the fourth diabatic surface), separate complete active space self-consistent field (CASSCF) calculations are performed over the complete range of geometries.

To obtain the three lowest nonrelativistic adiabatic PESs, the Hamiltonian in the diabatic basis is diagonalized. The relativistic spin−orbit coupling effects are included by using the formalism recently developed by Alexander, Manolopoulos, and Werner,[3] assuming the empirical value of the splitting parameters. The dependence of the PESs on the H_2 stretching coordinate is also incorporated and analyzed.

II. Computational Methods and Results

A. Geometries and Basis Sets. The Br−H_2 complex is described in Jacobi coordinates (R, r, θ). The R variable denotes the distance between the center of the H_2 monomer and the Br atom, and θ denotes the angle between the $\vec{R}$ vector and the H_2 bond axis. $\theta = 0°$ corresponds to the Br···H−H collinear arrangement. The H_2 monomer stretch is described by the r coordinate. Calculations were done for eight values of r ranging from 0.4 to 1.16 Å (the equilibrium distance r_e = 0.7408 Å included). Distance R ranged from 1.5 to 10.0 Å. The origin of the system of coordinates was placed at the center of the H_2 molecule. In the calculations of the diabatic energies, the H_2 molecule was located along the x axis, and the z axis was perpendicular to the triatomic plane. Calculations employed the augmented correlation-consistent polarized basis sets of quadruple-ζ quality (aug-cc-pvqz) basis function set of Dunning et al.[17−19] CCSD(T) calculations (but not CASSCF ones) also included bond functions, with the exponents: *sp* 0.9, 0.3, 0.1; *d* 0.6, 0.2,[20] in the form of a set: [3*s*3*p*2*d*], denoted as (332). Bond functions were centered in the middle of the $\vec{R}$ vector. Bond functions have been shown[21] to be both effective and economical for a number of van der Waals complexes including those with an open-shell moiety.[22−25]

B. Ab Initio Adiabatic and Diabatic Potential Energy Surfaces. The CC-M potentials are built in three steps:

1. Accurate CCSD(T) calculations are performed for the C_{2v} and $C_{\infty v}$ geometries, with a large basis set, to obtain benchmark interaction energies, see section 2.3. The model diabats for the C_s-symmetry geometries are obtained by a simple Legendre-polynomial interpolation between the C_{2v} and $C_{\infty v}$ geometries.

2. CASSCF calculations are carried out to obtain a nonadiabatic coupling (off-diagonal derivative) matrix element, mixing angle (Figure 1), and the fourth diabatic (off-diagonal) surface, see section 2.4.

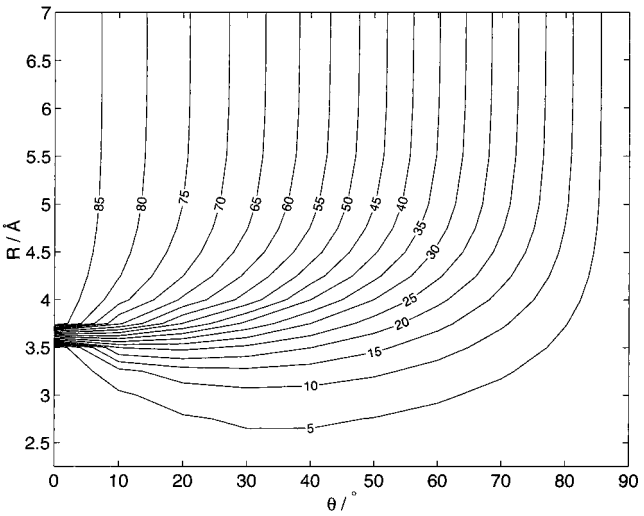

Figure 1. Contour plot of the γ_R mixing angle calculated in aug-cc-pvqz basis set, $r = r_e$.

3. The adiabatic PESs are obtained by diagonalizing the Hamiltonian matrix in terms of the diabatic basis set. See section 2.5.

All ab initio calculations reported in this paper were performed using the MOLPRO package.[26] The supermolecular method is used to calculate the interaction energies for the C_{2v} and $C_{\infty v}$ arrangements. This method derives the interaction energy as the difference between the energies of the dimer AB and the monomers A and B

$$\Delta E^{(n)} = E_{AB}^{(n)} - E_A^{(n)} - E_B^{(n)} \quad (1)$$

The superscript (n) denotes the level of ab initio theory. In the CCSD(T) calculations, the use of the above equation is straightforward and free from arbitrary choices, as long as the dimer and monomer energies are calculated with the same dimer centered basis set to counterpoise the basis set extension effect.[27] The CCSD(T) method is well-known to be very effective in recovering electron correlation effects in van der Waals complexes[28,29] and is preferred as long as the single-reference approach is valid. The variant of CCSD(T), R−UCCSD(T), is used, based on restricted open-shell Hartree−Fock (ROHF) orbitals, but with spin contamination allowed in the linear terms of the wave function.[30−32] Only valence electrons are correlated.

To calculate the off-diagonal matrix element of the Hamiltonian matrix, the CASSCF method is used (see section 2.4).

C. Model Diabatic PESs. The CCSD(T) approach can provide us with very accurate results, close to saturation with respect to basis set and correlation effects. Not only can this method be used with confidence for the lowest state of a given symmetry but also for excited states that are adequately represented by a single Slater determinant, e.g., when the excited state is related to a single-electron promotion from one p orbital to another, orthogonal p orbital. The latter feature was exploited in our recent study of the HCl−Cl van der Waals complex,[33] where two A′ states in the van der Waals region were well separated in a wide range of geometries. However, whereas formally the situation in the H_2−Br(^{2}P) case is identical, the H_2 molecule produces a much smaller splitting of the ^{2}P state of Br, and related hypersurfaces of the complex, and a significant nonadiabatic mixing of two adiabatic A′ states takes place, which

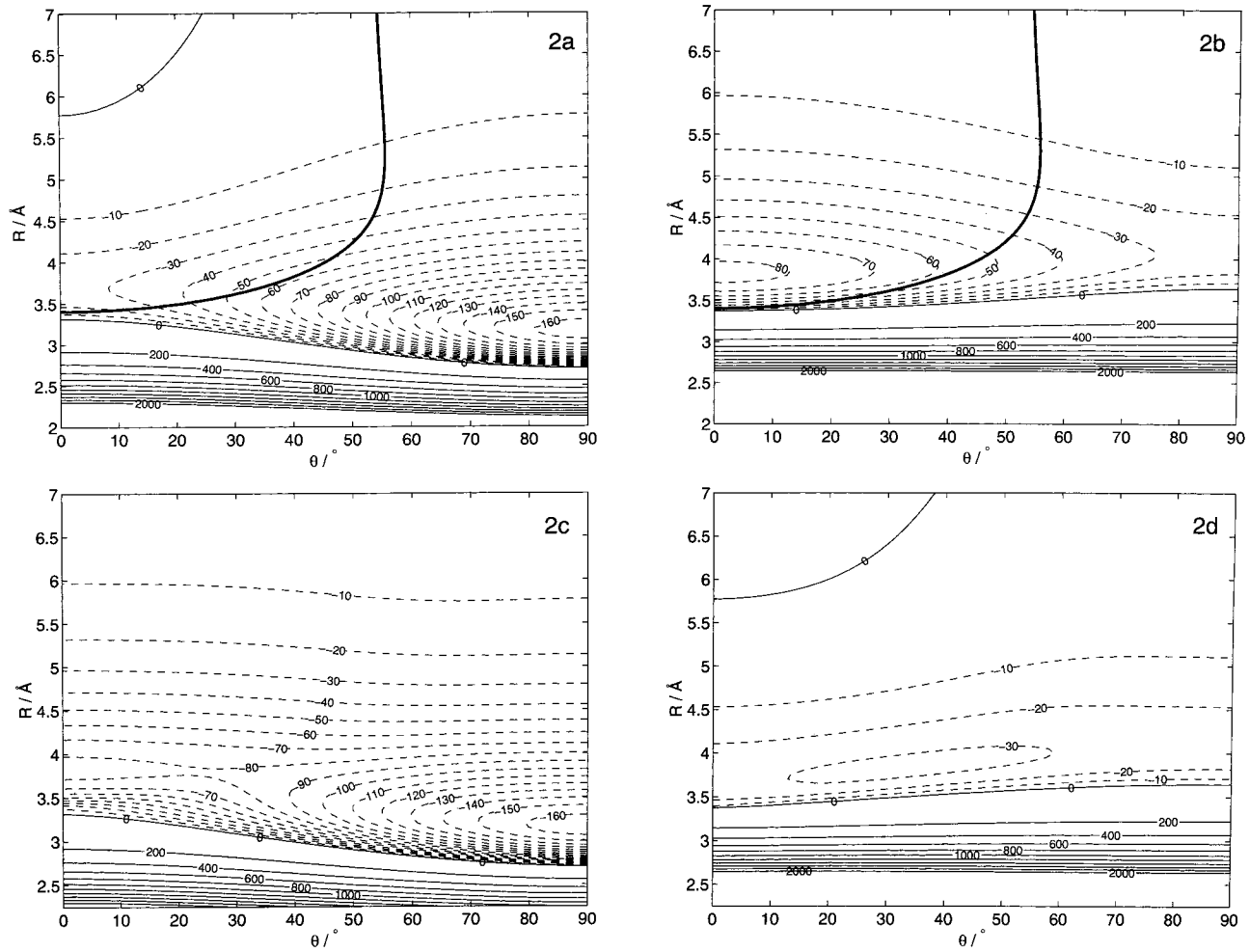

Figure 2. Contour plots of the modeled diabats and adiabats: (a) H_{11}^{CC-M} diabat, (b) H_{22}^{CC-M} diabat, (c) $1A'_{CC-M}$ adiabat and (d) $2A'_{CC-M}$ adiabat. Values in cm^{-1}, $r = r_e$.

culminates in the conical intersection for the collinear arrangement. This fact precludes the application of the CCSD(T) ansatz.

In previous work on Cl−H_2[2,4] and F−H_2,[1,3,34] the diabatic surfaces revealed a simple and regular shape. For a given R, the θ dependence was smooth and monotonic between the C_{2v} and $C_{\infty v}$ geometries. On this basis, we proposed the CC-M method which assumed the CCSD(T) interaction energies for the C_{2v} and $C_{\infty v}$ geometries and derived the interaction energies for the C_s geometries from the Legendre expansion truncated at $L = 2$, which is equivalent to the following angular dependence:

$$H_{11}^{CC-M}(R, r, \theta) = V_{A_1}^{CCSD(T)}(R, r) \sin^2 \theta + V_{\Sigma}^{CCSD(T)}(R, r) \cos^2\theta \quad (2)$$

$$H_{22}^{CC-M}(R, r, \theta) = V_{B_2}^{CCSD(T)}(R, r) \sin^2 \theta + V_{\Pi}^{CCSD(T)}(R, r) \cos^2\theta \quad (3)$$

$$H_{33}^{CC-M}(R, r, \theta) = V_{B_1}^{CCSD(T)}(R, r) \sin^2 \theta + V_{\Pi}^{CCSD(T)}(R, r) \cos^2\theta \quad (4)$$

The CC-M method was carefully verified by comparison with the scaled multireference configuration interaction results.[1,2] Ab initio CCSD(T) results for the A_1, B_1, and B_2 representations of the C_{2v} symmetry and Σ^+ and Π representations for the $C_{\infty v}$ symmetry have been fitted to analytic expressions to represent $V_X^{CCSD(T)}(R, r)$ in eqs 2−4. We use the analytic expression based on the Taylor expansion in the r coordinate with additional exponential r-dependent terms and the R dependence is of the Esposti−Werner[35] type:

$$V(R, r) = \left[G(R)e^{-a_1(R-a_2)-b_1\xi-b_2\xi^2} - T(R)\sum_{i=5}^{9}\frac{C_i}{R^i}\right]H(\xi) \quad (5)$$

where

$$G(R) = \sum_{j=0}^{8} g_j R^j \quad (6)$$

$$H(\xi) = \sum_{m=0}^{2} h_m \xi^m, \quad \xi = \frac{r - r_e}{r_e} \quad (7)$$

and damping function

$$T(R) = \frac{1}{2}(1 + \tanh(t_1 + t_2 R)) \quad (8)$$

FORTRAN codes generating PES are available on request from J. Kłos.

The contour plots of H_{11}^{CC-M} and H_{22}^{CC-M} for $r = 0.7408$ Å are shown in Figure 2 parts a and b, respectively. The contour

plot of the H_{33}^{CC-M} diabat is very similar to that in Figure 2b. In Figures 2 parts a and b, the bold line indicates the crossing of diabats, H_{11}^{CC-M}=H_{22}^{CC-M}. It originates at the region of $\Sigma^+ - \Pi$ conical intersection, at $\theta = 0°$).

D. CASSCF Calculations and Fitting of Fourth Diabatic Potential. *1. CASSCF Calculations.* The state averaged CASSCF orbitals are allowed for all three states, 1A′, 2A′, and 1A″.[36,37] The Br-moiety-related 1s orbital was kept frozen, the 2s, 2p, 3s and 3p orbitals were doubly occupied, and the 4s and 4p orbitals were active. The σ_g and σ_u^* molecular orbitals of hydrogen were also included in the active space.

Calculations were performed for several values of interhydrogen distance r and in a wide range of R and θ variables. These calculations require neither the self-consistency corrections nor the counterpoise correction. The basis set has been a bare aug-cc-pvqz set (without bond functions).

2. Diabatic Transformation. Diabatic surfaces provide more convenient representations for simulations of the van der Waals spectra of the system. These potentials contain information about couplings between the adiabatic wave functions of the same symmetry. The adiabatic-diabatic transformation yields diabatic states for which the nonadiabatic coupling matrix elements approximately vanish. The diabatic states are related to adiabatic states by a orthogonal transformation[38,39]

$$\begin{bmatrix}\Psi_1^d\\ \Psi_2^d\\ \Psi_3^d\end{bmatrix} = \begin{bmatrix}\cos\gamma & \sin\gamma & 0\\ -\sin\gamma & \cos\gamma & 0\\ 0 & 0 & 1\end{bmatrix}\begin{bmatrix}\Psi_2^a\\ \Psi_2^a\\ \Psi_3^a\end{bmatrix} \tag{9}$$

where the transformation angle γ depends on the nuclear coordinates. The resulting diabatic wave functions are no longer eigenstates of the electronic Hamiltonian. The Hamiltonian in the diabatic (p_x, p_y, p_z) basis is not diagonal, and the matrix elements are modeled as

$$H_{11} = H_{11}^{CC-M}$$

$$H_{22} = H_{22}^{CC-M}$$

$$H_{33} = H_{33}^{CC-M}$$

$$H_{12} = \sqrt{2}(E_{1A'}^{CAS} - E_{2A'}^{CAS})\cos\gamma\sin\gamma \tag{10}$$

The transformation angle γ, the so-called "mixing angle", is defined as the angle between the vector of the singly occupied p orbital and the $\vec{R}$ vector. It is a function of the Jacobi coordinates of the system. Within a two-state model, the mixing angle can, in principle, be obtained by the numerical integration of the nonadiabatic coupling matrix elements (NACMEs). To calculate the mixing angle, we used the method which maximizes the overlap with orbitals of the reference geometry.[40] The reference geometry is taken to be a collinear one for large intermolecular distances. This choice of reference geometry ensures that diabatic states coincide with adiabatic ones. This method calculates NACME in an approximate way using two slightly displaced geometries and the method of finite differences. Because it is convenient to perform a diabatic transformation in a system of coordinates with one axis along the $\vec{R}$ vector, the actual γ is redefined as

$$\gamma_R = \gamma + \theta - \frac{\pi}{2} \tag{11}$$

The plot of γ_R values is shown in Figure 1. This figure distinctly exhibits the region where the A′ states avoid crossing each other and the point where the Σ^+ and Π states cross. This is the region where the mixing is the strongest and the angle in eq 9 reaches 45°. The conical intersection occurs at Br···H−H, $\theta = 0°$, $R \approx 3.4$ Å. The intersection is related to the crossing of the Σ^+ and Π states.

TABLE 1: Stationary Points of Modeled Diabatic Surfaces for $r = r_e = 0.7408$ Å

diabat	D_e/cm^{-1}	R_e/Å	θ_e	type
H_{11}^{CC-M}	165.1	3.15	90	minimum
	28.2	3.70	0	saddle point
H_{22}^{CC-M}	83.1	3.85	0	minimum
	27	4.15	90	saddle point
H_{33}^{CC-M}	83.1	3.85	0	minimum
	38.2	4.00	90	saddle point

3. 3-D Fitting. To fit the three-dimensional set of ab initio data for H_{12} we used an analytical expression based on the expansion in associated Legendre functions P_l^1 and the Taylor expansion around $r = r_e$ interhydrogen distance

$$H_{12}(r, R, \theta) = V_{sh}(r, R, \theta) + V_{as}(r, R, \theta) \tag{12}$$

where

$$V_{sh}(r, R, \theta) = \sum_{l=1}^{6}\sum_{i=0}^{3}\sum_{j=0}^{3} g_{lj}c_i R^j \xi^i e^{\sqrt{1/2}(a-bR)-c\xi-d\xi^2}\sqrt{\frac{4l+1}{2}}P_{2l}^1(\cos\theta) \tag{13}$$

and

$$V_{as}(r, R, \theta) = \sum_{n=5}^{7}\sum_{i=0}^{3} c_i\xi^i\frac{C_n}{R^n}\sqrt{\frac{2(n-4)+1}{2}}P_{2(n-4)}^1(\cos\theta), \quad \xi = \frac{r - r_e}{r_e} \tag{14}$$

The fit contains 35 optimized parameters. Its quality can be expressed in terms of the root-mean-square value of 3.7 cm^{-1}. The biggest relative error equals approximately 20%, but for small values of energy, it is on the order of 1 cm^{-1}. Most of the relative errors are within the range of 2−8%.

E. Model Nonrelativistic Adiabatic PESs. To obtain the adiabatic counterparts of the diabatic surfaces, the diabatic matrix

$$\mathbf{H}^{el} = \begin{bmatrix}H_{11} & H_{12} & 0\\ H_{12} & H_{22} & 0\\ 0 & 0 & H_{33}\end{bmatrix} \tag{15}$$

is diagonalized. The global minima and stationary points of the modeled diabatic and adiabatic surfaces are shown in Table 1. The contour plots of 1A′ and 2A′ adiabatic surfaces for $r = r_e$ are shown in Figure 2 parts c and d, respectively.

III. Effect of H_2 Stretch

In Figures 3 and 4, we show R- and r-dependent contour plots of $V(R, r)$ for the $C_{\infty v}$ symmetry (the Σ^+ and Π states, Figure 3 parts a and b, respectively) and for the C_{2v} symmetry (the A_1, B_1, and B_2 states, Figure 4 parts a−c, respectively). One can see that the A_1 and Σ^+ potentials, which define the ground adiabatic state, are the most sensitive functions of r, whereas the other $V(R, r)$ potentials only weakly depend on r. The V_Σ potential reveals a shallow van der Waals minimum for large

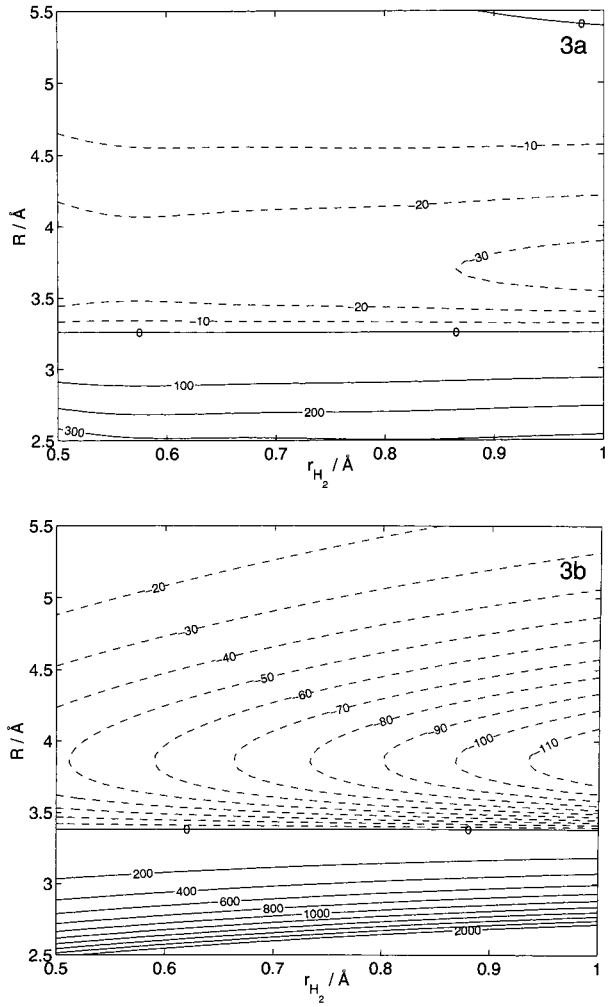

Figure 3. (*R*,*r*) dependence of interaction energies of (a) Σ and (b) Π symmetry. Values in cm^{-1}.

values of *R*, with *r* close to r_e and shorter, and has a large well for small values of *R* and large values of *r*, where the reaction region is reached. The V_{A1} potential for large *R* is everywhere attractive and fairly wide and flat with respect to *r*. On decreasing *R* and for small *r*, a repulsive bank emerges, whereas the attractive region is narrowed to larger *r* only, where the potential falls steeply into the reactive region.

The behavior of $V(R, r)$ determines the behavior of the diabats and adiabats according to eqs 2−4. The changes of *r* have the most significant impact on the H_{11} diabatic surface and only a mild effect on the other two, H_{22} and H_{33}. Compared with the plot for $r = r_e$ (Figure 2a) upon compressing H_2 to $r = 0.5292$ Å (Figure 5a), the T-shaped geometry minimum rises from −165 up to -97 cm^{-1}, whereas the collinear stationary point is slightly lowered (by a few cm^{-1}). In other words, the minimum energy path around Br is now shallower and flatter. By contrast, stretching H_2 to $r = 0.8466$ Å (Figure 5b) makes the T-shaped minimum deeper, from -165 down to -203 cm^{-1}.

The effect of stretching and compressing H_2 on the H_{22} and H_{33} diabats is minor, so we do not show it in the figures.

IV. Spin−Orbit Coupling and Model Relativistic Adiabatic PESs

Upon allowing for the spin−orbit coupling of the halogen atom, one obtains two atomic terms: $^2P_{3/2}$ and $^2P_{1/2}$, separated by $\Delta_{SO} = 3669.8$ cm^{-1}. The interaction with H_2 further splits the $^2P_{3/2}$ state into two states. To evaluate the resulting adiabatic

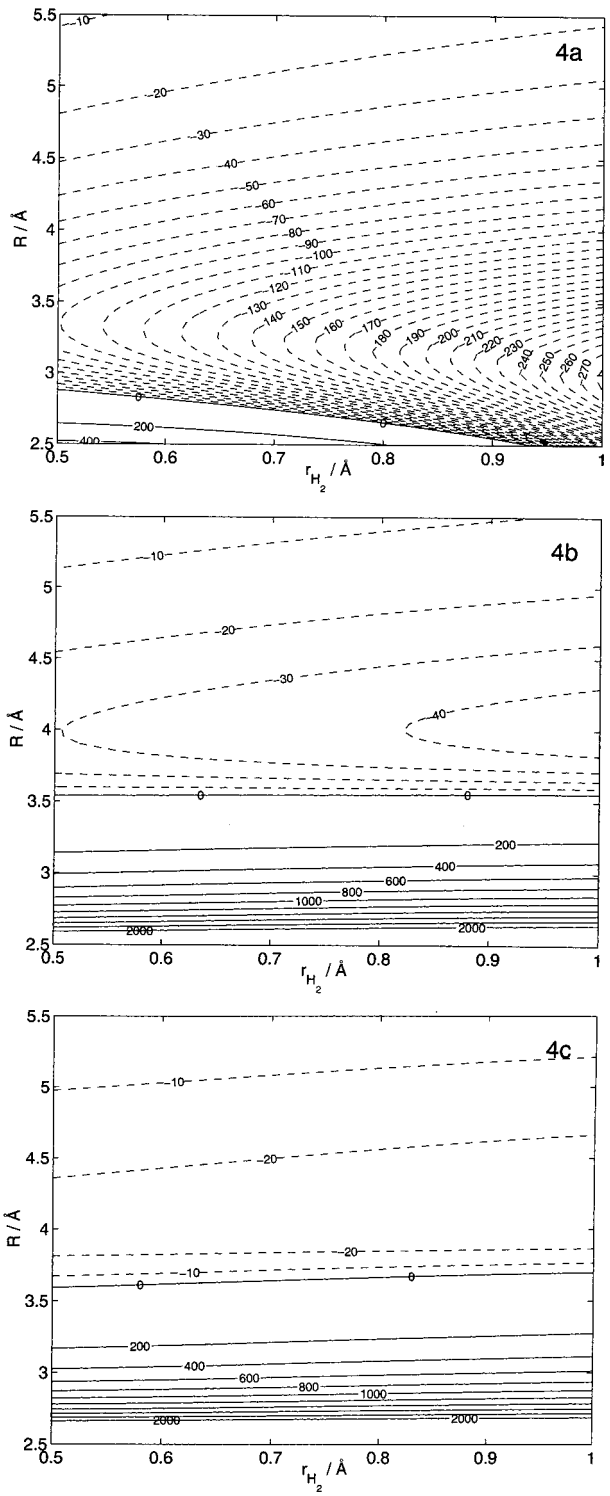

Figure 4. (*R*,*r*) dependence of interaction energies of (a) A_1, (b) B_1, and (c) B_2 symmetries. Values in cm^{-1}.

potential energy surfaces, we use the procedure described by Alexander, Manolopoulos, and Werner.[3] The matrix of the electrostatic interaction plus the spin−orbit Hamiltonian is expressed in the basis set invariant to time reversal (see ref 3 for details). Then the total matrix decouples

$$\mathbf{H}^{el} + \mathbf{H}^{SO} = \begin{bmatrix} \mathbf{H} & 0 \\ 0 & \mathbf{H}^{\dagger} \end{bmatrix} \tag{16}$$

where **H** is the 3 × 3 Hermitian matrix

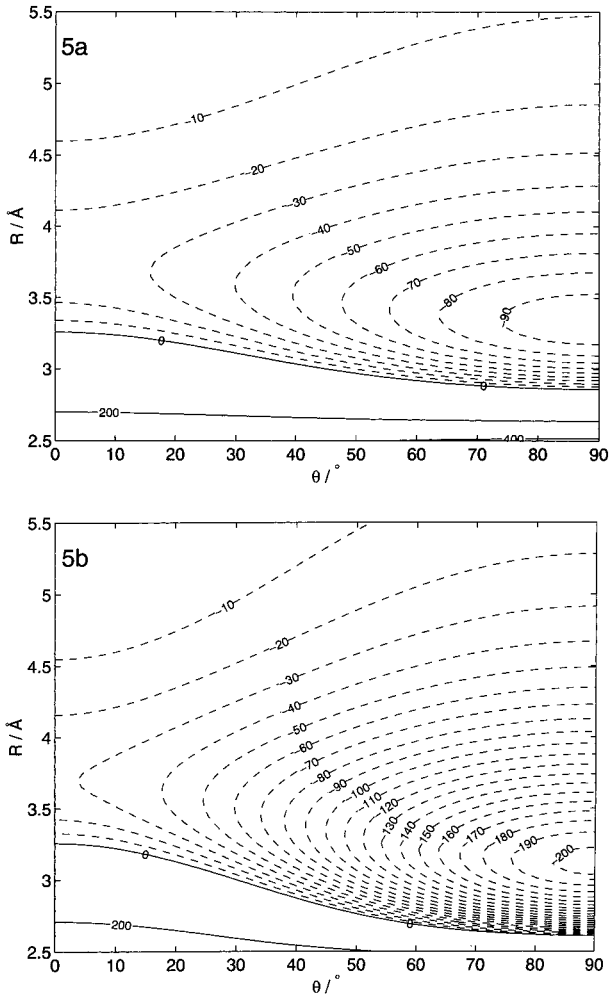

Figure 5. Contour plots of the modeled H_{11}^{CC-M} diabat for (a) r = 0.529 177 Å and (b) r = 0.846 683 Å. Values in cm^{-1}.

$$\mathbf{H} = \begin{bmatrix} H_{11} - V_1 - i\sqrt{2}B & V_1 & \\ & V_\Pi + A & V_2 \\ & & V_\Pi - A \end{bmatrix} \tag{17}$$

where $V_1 = H_{12}$, $V_\Pi = (H_{33} + H_{22})/2$, and $V_2 = (H_{33} - H_{22})/2$. A and B are spin−orbit matrix elements:

$$A \equiv i\langle \Pi_y | H^{SO} | \Pi_x \rangle \tag{18}$$

and

$$B \equiv \langle \bar{\Pi}_x | H^{SO} | \Sigma \rangle \tag{19}$$

where, after Alexander et al.,[3] we used the compact Cartesian notation for diabatic states: $|\Pi_x\rangle$, $|\Pi_y\rangle$, and $|\Sigma\rangle$, related to the projections of the electronic orbital and spin momenta along the vector $\vec{R}$. The bar above the $|\Pi_x\rangle$ state in Eq. 19 denotes β spin. On diagonalizing the matrix in eq 17, three adiabatic potential energy surfaces are obtained, shown in Figure 6 parts a−c. They are numbered in the order of increasing energy. In the limit of large R, the first two adiabatic PESs correlate with the $^2P_{3/2}$ state of Br, with the projection of j upon the b$\vec{R}$ vector equal to 3/2 for the ground state and 1/2 the first excited state. The third adiabat (Figure 6c) correlates with the $^2P_{1/2}$ term of the Br atom.

One can see that the relativistic adiabatic surfaces significantly differ from nonrelativistic ones. The lowest adiabatic surface

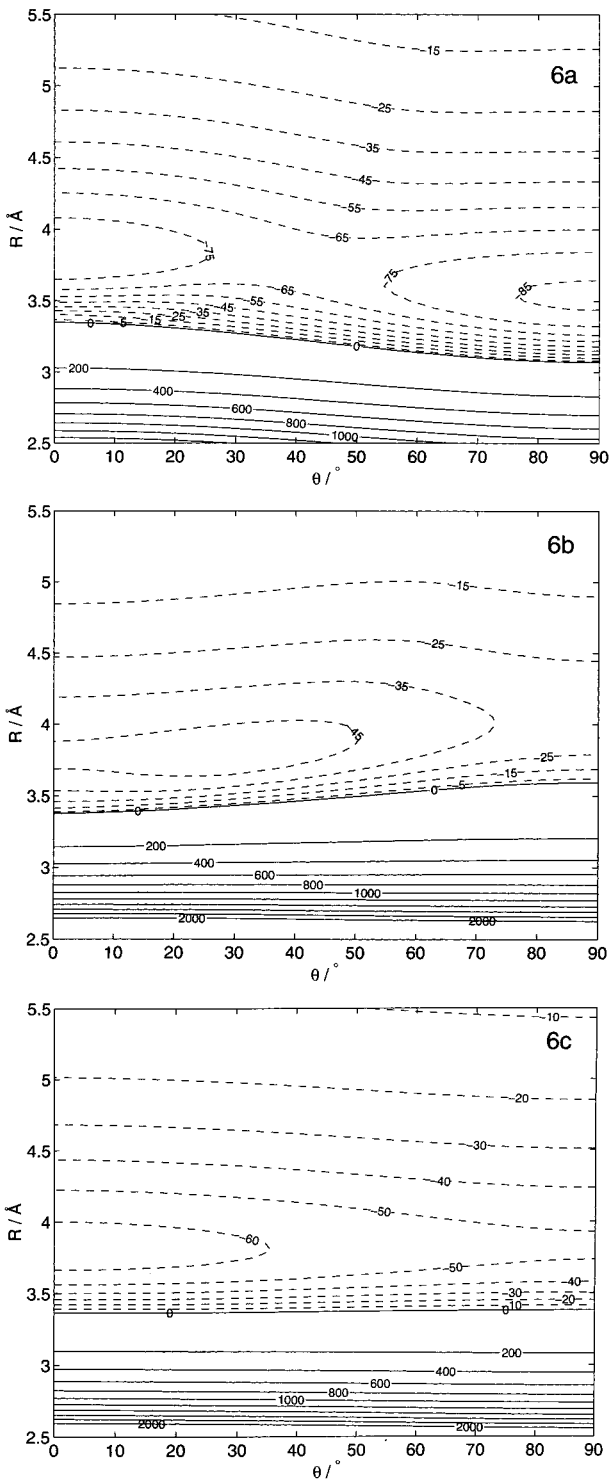

Figure 6. Contour plots of the spin−orbit corrected adiabats. (a) adiabat 1, which correlates with Br($^2P_{3/2}$), (b) adiabat 2, which correlates with Br($^2P_{3/2}$), and (c) adiabat 3, which correlates to Br($^2P_{1/2}$). Values in cm^{-1}, $r = r_e$.

is now half as deep at the T-shaped minimum (D_e = 87 cm^{-1}), and considerably flattened with a 17 cm^{-1} barrier for the H_2 rotation, around 40°, and another local minimum for the collinear arrangement (D_e = 83 cm^{-1}). The other adiabatic surface related to the same $^2P_{3/2}$ asymptotic limit is shallower, with a maximum at 90° and a minimum at 0° with the well depth of 46 cm^{-1}. The third state, asymptotically separated by the 3669.8 cm^{-1} SO coupling, resembles the second in shape but is slightly deeper.

TABLE 2: Stationary Points of Modeled Spin−Orbit Corrected Adiabatic Surfaces for $r = r_e = 0.7408$ Å

adiabat	D_e/cm^{-1}	R_e/Å	θ_e	type
adiabat 1	87	3.55	90	minimum
adiabat 1	83	3.85	0	minimum
adiabat 2	49	3.80	30	minimum
adiabat 2	46	3.80	0	saddle
adiabat 2	32	4.05	90	saddle
adiabat 3	64	3.80	0	minimum
adiabat 3	51	3.85	90	saddle

The D_e and R_e parameters of the three adiabatic PESs are listed in Table 2.

V. Summary and Conclusions

The 3-D CC-M diabatic potentials for the first three states of the H_2−Br complex have been derived from ab initio calculations for the T-shaped and collinear forms at the CCSD-(T) level of theory with a large basis set. It has been found that the ground state is sensitive to the changes of r. In particular, the height of the barrier decreases by stretching the H_2 molecule and increases by compressing it.

The ground state 1A′ PES of H_2−Br may be compared with the ground state 1A′ PES of H_2−Cl which was derived recently by us within the same CC-M framework.[2] The intermediate and long range of these surfaces are similar, with the H_2−Cl van der Waals well being almost of the same well depth, and with almost the same hindrance for the H_2 rotation of ca. 82 cm^{-1}.

The characteristics of the PESs are dramatically changed upon allowing for the spin−orbit effects. The relativistic ground-state adiabatic PES is half as deep as the nonrelativistic one, 87 vs 165 cm^{-1}, and the barrier to the rotation of H_2 is shifted toward 40° and lowered from 82 to 17 cm^{-1}, whereas the collinear saddle point transforms into a minimum. The second and third adiabatic surfaces are also considerably flattened. These results qualitatively agree with the finding of Alexander, Manolopoulos, and Werner[3] for F + H_2 in that the "spin−orbit coupling cannot be neglected in the region of the van der Waals minimum [...] and significantly alters both the depth and position of the van der Waals well".

We also checked the influence of the electronic correlation of the inner shells of the Br atom on the interaction energy of the A_1 state in the global minimum. Upon setting active space to include the 1s, 2s, and 2p orbitals frozen, the 3s, 3p, 3d, 4s, $4p_x$, and $4p_y$ doubly occupied, and $4p_z$ active, the interaction energy increased to 167.7 cm^{-1}. The difference with the default (1s, 2s, 3s, 3p, and 3d orbitals frozen, 4s, $4p_x$ and $4p_y$ doubly occupied, and $4p_z$ active) active space is 2.7 cm^{-1}, so it is less than 2%.

Finally, it is worthwhile to stress that our CC-M approach is expected to provide reliable PESs for other atom−H_2 complexes as well, which are in the entry channels of many reactions, such as O + H_2, N + H_2, S + H_2, etc. Recently, a similar approach has been successfully adapted to the van der Waals system Cl-(^{2}P) + CH_4[41] which is even more challenging. The expansion of the anisotropy of the Cl(^{2}P) + CH_4 system was done in spherical harmonics adapted to the tetrahedral symmetry of the problem.

Acknowledgment. M.M.S. and G.C. thank the National Science Foundation (Grant No. CHE-0078533) for its support. International collaboration was supported by NATO through the Linkage Grant CRG.LG 974215. J.K. and G.C. acknowledge support by the Polish Committee for Scientific Research KBN (Grant 3 T09A 112 18).

References and Notes

(1) Kłos, J.; Chałasiński, G.; Szczęśniak, M. M. *Int. J. Quantum Chem.* In press.
(2) Kłos, J.; Chałasiński, G.; Szczęśniak, M. M. *J. Chem. Phys.* In press.
(3) Alexander, M. H.; Manolopoulos, D. E.; Werner, H.-J. *J. Chem. Phys.* **2000**, *113*, 11084.
(4) Bian, W.; Werner, H.-J. *J. Chem. Phys.* **2000**, *112*, 220.
(5) Mielke, S. L.; Tawa, G. J.; Truhlar, D. G.; Schwenke, D. *Chem. Phys. Lett.* **1995**, *234*, 57.
(6) Mielke, S. L.; Truhlar, D. G.; Schwenke, D. *J. Phys. Chem.* **1995**, *99*, 16210.
(7) Volobuev, Y. L.; Hack, M. D.; Truhlar, D. G. *J. Phys. Chem. A* **1999**, *103*, 6255.
(8) Aquilanti, V.; Cavalli, S.; Pirani, F.; Volpi, A.; Cappelletti, D. *J. Phys. Chem. A* **2001**, *105*, 2401.
(9) Skouteris, D.; Manolopoulos, D. E.; Bian, W.; Werner, H. J.; Lai, L.-H.; Liu, K. *Science* **1999**, *286*, 1713.
(10) Loomis, R. A.; Lester, M. I. *Annu. Rev. Phys. Chem.* **1997**, *48*, 643.
(11) Marshall, M. D.; Pond, B.; Hopman, S.; Lester, M. *J. Chem. Phys.* **2001**, *114*, 7001.
(12) Nesbitt, D. J.; Leone, S. R. *J. Chem. Phys* **1980**, *73*, 6182.
(13) Takayanagi, T.; Kurosaki, Y. *J. Chem. Phys* **2000**, *112*, 7158.
(14) Krems, R. V.; Buchachenko, A. A. *J. Phys. B* **2000**, *33*, 4551.
(15) Krems, R. V.; Buchachenko, A. A.; Szczęśniak, M. M.; Kłos, J.; Chałasiński, G. *J. Chem. Phys.* **2002**, *116*, 1457.
(16) Kłos, J.; Chałasiński, G.; Krems, R. V.; Buchachenko, A. A.; Aquilanti, V.; Pirani, F.; Cappelletti, D. *J. Chem. Phys.* **2002**, *116*, 9269.
(17) Dunning, T. H., Jr. *J. Chem. Phys.* **1989**, *90*, 1007.
(18) Kendall, R. A.; Dunning, T. H., Jr.; Harrison, R. J. *J. Chem. Phys.* **1992**, *96*, 6796.
(19) Woon, D. E.; Dunning, T. H., Jr. *J. Chem. Phys.* **1993**, *98*, 1358.
(20) Tao, F.-M.; Pan, Y.-K. *J. Chem. Phys.* **1992**, *97*, 4989.
(21) Burcl, R.; Chałasiński, G.; Bukowski, R.; Szczęśniak, M. M. *J. Chem. Phys.* **1995**, *103*, 1498.
(22) Cybulski, S. M.; Kendall, R. A.; Chałasiński, G.; Severson, M. W.; Szczęśniak, M. M. *J. Chem. Phys.* **1997**, *106*, 7731.
(23) Kendall, R. A.; Chałasiński, G.; Kłos, J.; Bukowski, R.; Severson, M. W.; Szczęśniak, M. M.; Cybulski, S. M. *J. Chem. Phys.* **1998**, *108*, 3235.
(24) Cybulski, S. M.; Burcl, R.; Chałasiński, G.; Szczęśniak, M. M. *J. Chem. Phys.* **1995**, *103*, 10116.
(25) Cybulski, S. M.; Toczyłowski, R. *J. Chem. Phys.* **1999**, *111*, 10520.
(26) MOLPRO is a package of ab initio programs written by H.-J. Werner and P. J. Knowles, with contributions from R. D. Amos, A. Bernhardsson, A. Berning, P. Celani, D. L. Cooper, M. J. O. Deegans, A. J. Dobbyn, F. Eckert, C. Hampel, G. Hetzer, T. Korona, R. Lindh, A. W. Lloyd, S. J. McNicholas, F. R. Manby, W. Meyer, M. E. Mura.; Nicklass, A.; Pitzer, P. P. R.; Rauhut, G.; Schütz, M.; Stoll, H.; Stone, A. J.; Tarroni, R.; Thorsteinsson., T.
(27) Boys, S. F.; Bernardi, F. *Mol. Phys.* **1970**, *19*, 553.
(28) Chałasiński, G.; Szczęśniak, M. M. *Chem. Rev.* **1994**, *94*, 1723.
(29) Chałasiński, G.; Szczęśniak, M. M. *Chem. Rev.* **2000**, *100*, 4253.
(30) Knowles, P. J.; Hampel, C.; Werner, H.-J. *J. Chem. Phys.* **1993**, *99*, 5219.
(31) Scuseria, G. *Chem. Phys. Lett.* **1991**, *176*, 27.
(32) Rittby, M.; Bartlett, R. *J. Phys. Chem.* **1988**, *92*, 3033.
(33) Kłos, J.; Chałasiński, G.; Szczęśniak, M. M.; Werner, H.-J. *J. Chem. Phys.* **2001**, *115*, 3085.
(34) Stark, K.; Werner, H.-J. *J. Chem. Phys.* **1996**, *104*, 6515.
(35) Esposti, A. D.; Werner, H.-J. *J. Chem. Phys.* **1990**, *93*, 3351.
(36) Werner, H.-J.; Knowles, P. J. *J. Chem. Phys.* **1985**, *82*, 5053.
(37) Knowles, P. J.; Werner, H.-J. *Chem. Phys. Lett.* **1985**, *115*, 259.
(38) Werner, H.-J.; Follmeg, B.; Alexander, M. H. *J. Chem. Phys.* **1988**, *89*, 3139.
(39) Alexander, M. H. *J. Chem. Phys.* **1993**, *99*, 6014.
(40) Simah, D.; Hartke, B.; Werner, H.-J. *J. Chem. Phys* **1999**, *111*, 4523.
(41) Kłos, J. *Chem. Phys. Lett.* **2002**, *359*, 309.